Journal of Solid State Chemistry 182 (2009) 1075–1081

Contents lists available at ScienceDirect

Journal of Solid State Chemistry

journal homepage: www.elsevier.com/locate/jssc

Syntheses, structures, magnetism, and optical properties of gadolinium scandium chalcogenides

Geng Bang Jin [a,b], Eun Sang Choi [c], Thomas E. Albrecht-Schmitt [a,b,*]

[a] Department of Civil Engineering and Geological Sciences, University of Notre Dame, Notre Dame, IN 46556, USA
[b] Department of Chemistry and Biochemistry, University of Notre Dame, Notre Dame, IN 46556, USA
[c] National High Magnetic Field Laboratory, Florida State University, Tallahassee, FL 32310, USA

ARTICLE INFO

Article history:
Received 10 November 2008
Received in revised form
26 January 2009
Accepted 1 February 2009
Available online 12 February 2009

Keywords:
Interlanthanide chalcogenide
Mixed-lanthanide chalcogenide
Lanthanide magnetism

ABSTRACT

Three gadolinium scandium chalcogenides have been synthesized using Sb_2Q_3 (Q = S, Se) fluxes at 975 °C. $Gd_{3.04}Sc_{0.96}S_6$, $GdScS_3$, and $Gd_{1.05}Sc_{0.95}Se_3$ are crystallized in U_3ScS_6 type, $GdFeO_3$ type, and $UFeS_3$ type structures, respectively. The magnetic susceptibilities for these compounds follow the Curie–Weiss law above their transition temperatures. The effective magnetic moments are close to calculated values for free Gd^{3+} ions. The Weiss constants for $Gd_{3.04}Sc_{0.96}S_6$, $GdScS_3$, and $Gd_{1.05}Sc_{0.95}Se_3$ are determined to be −3.3(1), −4.5(4), and 1.5(1) K, respectively. $Gd_{3.04}Sc_{0.96}S_6$ orders antiferromagnetically below 9 K. $GdScS_3$ exhibits an antiferromagnetic ordering below 3 K with a weak ferromagnetism. $Gd_{1.05}Sc_{0.95}Se_3$ undergoes a ferromagnetic transition around 5 K. The optical band gaps for $Gd_{3.04}Sc_{0.96}S_6$, $GdScS_3$, and $Gd_{1.05}Sc_{0.95}Se_3$ are 1.5, 2.1, and 1.2 eV, respectively.

1. Introduction

Ternary interlanthanide chalcogenide systems were extensively studied more than two decades ago [1–13]. This initial work was more focused on determining the compositions and structures of these compounds. Recently, a large number of new compounds including quaternary phases [14] have been prepared using a variety of fluxes [14–23]. The physical properties of many of these compounds are well-developed. In addition to their diverse structural chemistry and potentially tunable optical properties, the growing interest for interlanthanide chalcogenides comes from their various magnetic properties due to the large and anisotropic magnetic moments of most of the lanthanide ions. However, like other lanthanide compounds, studying the nature and magnitude of the coupling between magnetic ions in those compounds is not straightforward. The difficulty is mainly due to two effects: (1) crystal field splitting of the ground state for lanthanide ions with orbital contributions, e.g. Ce^{3+} and Yb^{3+} and (2) the thermal population of free ion excited states in cases of Sm^{3+} and Eu^{3+} [24,25]. In contrast, Gd^{3+} ion has a ground state of $^8S_{7/2}$, which is not perturbed by crystal field effects and is located at 10^{-4} cm^{-1} below the first excited state [25]. Therefore, gadolinium compounds are unique materials that can be used to reveal the nature of magnetic interactions between ions in interlanthanide chalcogenides structures.

The Sc^{3+} ion has very similar structural chemistry with lanthanides, and it is about 0.18 Å smaller in size than Gd^{3+} ion [26]. Gd/Sc/Q (Q = S, Se) compounds are expected to adopt ordered interlanthanide chalcogenides structures. Furthermore, Sc^{3+} ions will not interfere with the magnetic behavior of Gd^{3+} ions due to their [Ar] electronic configuration. Gd/Sc/Q system is the best candidate for the above purpose, even though it has been poorly studied. Rodier et al. identified a $GdScS_3$ phase [6] and a $Gd_3Sc_2S_7$ phase [8] from powder X-ray diffraction experiments.

In the present study, we successfully synthesized three gadolinium scandium chalcogenides ($Gd_{3.04}Sc_{0.96}S_6$, $GdScS_3$, and $Gd_{1.05}Sc_{0.95}Se_3$) using Sb_2Q_3 (Q = S, Se) fluxes. Their magnetic and optical properties are also investigated.

2. Experimental

2.1. Starting materials

Gd (99.9%, Alfa-Aesar), Sc (99.9%, Alfa-Aesar), S (99.5%, Alfa-Aesar), Se (99.5%, Alfa-Aesar), and Sb (99.5%, Alfa-Aesar) were used as received. The Sb_2Q_3 (Q = S, Se) fluxes were prepared from the direct reaction of the elements in sealed fused-silica ampoules at 850 °C.

2.2. Syntheses

For both reactions, 100 mg of Gd, Sc, and Q in a molar ratio of 1:1:3 were loaded into fused-silica ampoules with 60 mg of Sb_2Q_3

* Corresponding author. Fax: +1 574 631 9236.
E-mail address: talbrec1@nd.edu (T.E. Albrecht-Schmitt).

0022-4596/$ - see front matter © 2009 Elsevier Inc. All rights reserved.
doi:10.1016/j.jssc.2009.02.002

(Q = S, Se) in a glovebox filled with argon. The ampoules were flame sealed under vacuum and heated in programmable tube furnaces. The following heating profile was used: 2 °C/min to 500 °C (held for 1 h), 0.5 °C/min to 975 °C (held for 7 d), 0.04 °C/min to 550 °C (held for 2 d), and 0.5 °C/min to 24 °C. The products for the sulfide reaction include dark red needles of $Gd_{3.04}Sc_{0.96}S_6$ and brown prisms of $GdScS_3$ in high yields. $Gd_{3.04}Sc_{0.96}S_6$ can also be prepared using KI flux under the same reaction condition. Black needles of $Gd_{1.05}Sc_{0.95}Se_3$ were found as the major product in selenide reaction. Unreacted Sb_2Q_3 fluxes were present as large black chunks, which can be easily distinguished from title compounds. Single crystals of $Gd_xSc_yQ_z$ were isolated manually and ground for powder X-ray diffraction and physical property measurements. The purities of collected samples were confirmed by comparing the powder patterns calculated from the single crystal X-ray structures with the experimental data. Semi-quantitative SEM/EDX analyses were performed on several single crystals for each compound using a JEOL 840/Link Isis or JEOL JSM-7000F instruments. The presence of Gd, Sc, S, and Se were confirmed in corresponding samples. Sb was not detected in the crystals. All three compounds are air stable for a long period of time.

2.3. Crystallographic studies

Single crystals of $Gd_xSc_yQ_z$ (Q = S, Se) were mounted on glass fibers with epoxy and optically aligned on a Bruker APEX single crystal X-ray diffractometer using a digital camera. Initial intensity measurements were performed using graphite monochromated Mo $K\alpha$ ($\lambda = 0.71073$ Å) radiation from a sealed tube and monocapillary collimator. SMART (v 5.624) was used for preliminary determination of the cell constants and data collection control. The intensities of reflections of a sphere were collected by a combination of three sets of exposures (frames). Each set had a different ϕ angle for the crystal and each exposure covered a range of 0.3° in ω. A total of 1800 frames were collected with exposure times per frame of 10 or 20 seconds depending on the crystal.

For $Gd_xSc_yQ_z$ (Q = S, Se), determination of integrated intensities and global refinement were performed with the Bruker SAINT (v 6.02) software package using a narrow-frame integration algorithm. These data were treated first with a face-index numerical absorption correction using XPREP [27], followed by a semi-empirical absorption correction using SADABS [28]. The program suite SHELXTL (v 6.12) was used for space group determination (XPREP), direct methods structure solution (XS), and least-squares refinement (XL) [27]. The final refinements included anisotropic displacement parameters for all atoms and secondary extinction. Some crystallographic details are given in Table 1. Atomic coordinates and equivalent isotropic displacement parameters for $Gd_{3.04}Sc_{0.96}S_6$, $GdScS_3$, and $Gd_{1.05}Sc_{0.95}Se_3$ are given in Tables 2–4, respectively. Additional crystallographic details can be found in the Supporting information.

$Gd_{3.04}Sc_{0.96}S_6$, $GdScS_3$, and $Gd_{1.05}Sc_{0.95}Se_3$ are all crystallized in known ordered structures. Metal positions were easily assigned according to their atomic radii and refined anisotropically. However, a non-positive displacement ellipsoid was found for the octahedral-coordinate Sc(2) atom in $Gd_{3.04}Sc_{0.96}S_6$ and the thermal parameters for Sc(1) atom was relatively small. Disorder of Gd and Sc atoms on those sites were suspected considering Gd atom is much heavier than Sc atom. New refinement with disorder of Gd and Sc was carried out. This refinement resulted in normal thermal parameters for Gd4/Sc1 and Gd5/Sc2 positions and lowered the R_1 and R_w (defined in Table 1) values from 0.0202

Table 1
Crystallographic data for $Gd_xSc_yQ_z$ (Q = S, Se).

Formula	$Gd_{3.04}Sc_{0.96}S_6$	$GdScS_3$	$Gd_{1.05}Sc_{0.95}Se_3$
Formula weight	713.28	298.39	444.70
Color	Dark red	Brown	Black
Crystal system	Orthorhombic	Orthorhombic	Orthorhombic
Space group	*Pnnm* (No. 58)	*Pnma* (No. 62)	*Cmcm* (No. 63)
a (Å)	13.5488(8)	7.0361(6)	3.8922(4)
b (Å)	16.3057(10)	9.4574(8)	12.648(1)
c (Å)	3.8337(2)	6.3833(6)	9.621(1)
V (Å^3)	846.95(8)	424.77(6)	473.64(8)
Z	4	4	4
T (K)	193	193	193
λ (Å)	0.71073	0.71073	0.71073
ρ_{calcd} (g cm^{-3})	5.594	4.666	6.236
μ (cm^{-1})	256.00	183.22	387.87
$R(F)$[a]	0.0187	0.0168	0.0258
$R_w(F_o^2)$[b]	0.0466	0.0426	0.0681

[a] $R(F) = \sum ||F_o| - |F_c|| / \sum |F_o|$ for $F_o^2 > 2\sigma(F_o^2)$.
[b] $R_w(F_o^2) = [\sum[w(F_o^2 - F_c^2)^2] / \sum wF_o^4]^{1/2}$.

Table 2
Atomic coordinates, occupancies, and equivalent isotropic displacement parameters for $Gd_{3.04}Sc_{0.96}S_6$.

Atom (site)	x	y	z	Occupancy	U_{eq} (Å^2)[a]
Gd1	0.04635(2)	0.21946(2)	0	1	0.0068(1)
Gd2	0.74754(2)	0.60147(2)	0	1	0.0083(1)
Gd3	0.18363(2)	0.64970(2)	0	1	0.0072(1)
Gd4/Sc1	1/2	1/2	0	0.022(3)/0.978(3)	0.0075(5)
Gd5/Sc2	1/2	0	0	0.053(3)/0.947(3)	0.0075(5)
S1	0.0914(1)	0.92177(8)	0	1	0.0073(5)
S2	0.3785(1)	0.61084(9)	0	1	0.0073(5)
S3	0.39350(9)	0.25259(8)	0	1	0.0075(3)
S4	0.31342(9)	0.02225(8)	0	1	0.0080(3)
S5	0.0210(1)	0.39607(8)	0	1	0.0071(3)
S6	0.3143(1)	0.78930(8)	0	1	0.0070(3)

[a] U_{eq} is defined as one-third of the trace of the orthogonalized U_{ij} tensor.

Table 3
Atomic coordinates, occupancies, and equivalent isotropic displacement parameters for $GdScS_3$.

Atom (site)	x	y	z	Occupancy	U_{eq} (Å^2)[a]
Gd1	0.09845(3)	1/4	0.03744(4)	1	0.0099(1)
Sc1	0	0	1/2	1	0.0066(2)
S1	0.3151(1)	0.43309(8)	0.3248(1)	1	0.0086(2)
S2	0.9553(2)	1/4	0.6385(2)	1	0.0082(2)

[a] U_{eq} is defined as one-third of the trace of the orthogonalized U_{ij} tensor.

Table 4
Atomic coordinates, occupancies, and equivalent isotropic displacement parameters for $Gd_{1.05}Sc_{0.95}Se_3$.

Atom (site)	x	y	z	Occupancy	U_{eq} (Å^2)[a]
Gd1	0	0.74784(3)	1/4	1	0.0108(2)
Gd2/Sc1	0	0	0	0.052(4)/0.948(4)	0.0100(5)
Se1	0	0.35707(5)	0.06052(5)	1	0.0100(5)
Se2	0	0.08333(6)	1/4	1	0.0098(3)

[a] U_{eq} is defined as one-third of the trace of the orthogonalized U_{ij} tensor.

and 0.0512 to 0.0187 and 0.0466. The final occupancies of Gd4/Sc1 and Gd5/Sc2 sites are 0.022(3)/0.978(3) and 0.053(3)/0.947(3).

The refinements for $GdScS_3$ showed that the small metal position is occupied by Sc atom exclusively. Initial refinement for $Gd_{1.05}Sc_{0.95}Se_3$ resulted in small thermal parameters of the octahedral Sc atom as found similarly in case of $Gd_{3.04}Sc_{0.96}S_6$. Introducing disorder of Gd and Sc in the following refinement lowered the R_1 and R_w values from 0.0285 and 0.0769 to 0.0258 and 0.0681. The final occupancies of Gd2/Sc1 site is 0.052(4)/0.948(4). Similar disordered arrangements of Er and Sc atoms on octahedral sites have been observed in Er_3ScS_6 [6,9] and $Er_3Sc_2S_7$ [8] phases.

2.4. Powder X-ray diffraction

Powder X-ray diffraction patterns were collected with a Rigaku Miniflex powder X-ray diffractometer using Cu $K\alpha$ ($\lambda = 1.54056$ Å) radiation.

2.5. Magnetic susceptibility measurements

Magnetism data were measured on powders in gelcap sample holders with a quantum design PPMS 9 T magnetometer/susceptometer between 2 and 300 K and in applied fields up to 9 T. DC susceptibility measurements were made under zero-field-cooled conditions with an applied field of 0.1 T. Susceptibility values were corrected for the sample diamagnetic contribution according to Pascal's constants [29] as well as for the sample holder diamagnetism. Experimental effective magnetic moments and Weiss constants for $Gd_{3.04}Sc_{0.96}S_6$, $GdScS_3$, and $Gd_{1.05}Sc_{0.95}Se_3$ were obtained from extrapolations from fits between 100 and 300 K.

2.6. UV–vis–NIR Diffuse Reflectance Spectroscopy

The diffuse reflectance spectra for $Gd_xSc_yQ_z$ ($Q = S$, Se) were measured from 200 to 2500 nm using a Shimadzu UV3100 spectrophotometer equipped with an integrating sphere attachment. The Kubelka–Munk function was used to convert diffuse reflectance data to absorption spectra [30].

3. Results and discussion

3.1. Structures of $Gd_xSc_yQ_z$ ($Q = S, Se$)

$Gd_{3.04}Sc_{0.96}S_6$, $GdScS_3$, and $Gd_{1.05}Sc_{0.95}Se_3$ adopt U_3ScS_6 type [31], $GdFeO_3$ type [32], and $UFeS_3$ type [33] structures, respectively. These structure types are common ordered interlanthanide chalcogenides structure types that have been detailed in previous works [15,17,19]. The slight disorder of Gd/Sc in the six-coordinate cation positions within $Gd_{3.04}Sc_{0.96}S_6$ and $Gd_{1.05}Sc_{0.95}Se_3$ are omitted in the following discussion.

As shown in Fig. 1, $Gd_{3.04}Sc_{0.96}S_6$ has a very complex three-dimensional structure, which contains two bicapped trigonal prismatic Gd positions, one monocapped trigonal prismatic Gd position, and two octahedral Sc positions. The structure can be described as two-dimensional $[Gd_3S_6]^{3-}$ slabs extending in the [*ac*] plane with further connections at S(4) positions. Isolated one-dimensional edge-sharing ScS_6 octahedral chains running down the *c* axis fill the gaps between these slabs. These slabs are constructed from face-sharing and edge-sharing GdS_8 and GdS_7 polyhedra.

$GdScS_3$ is crystallized in a distorted perovskite type structure, which is depicted in Fig. 2. Each ScS_6 octahedron share corners

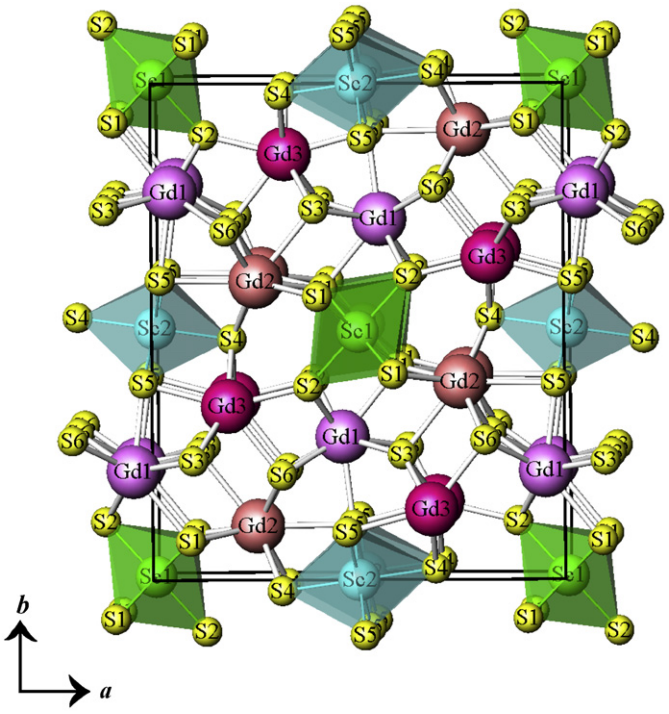

Fig. 1. A view of the three-dimensional structure of $Gd_{3.04}Sc_{0.96}S_6$ along the *c* axis.

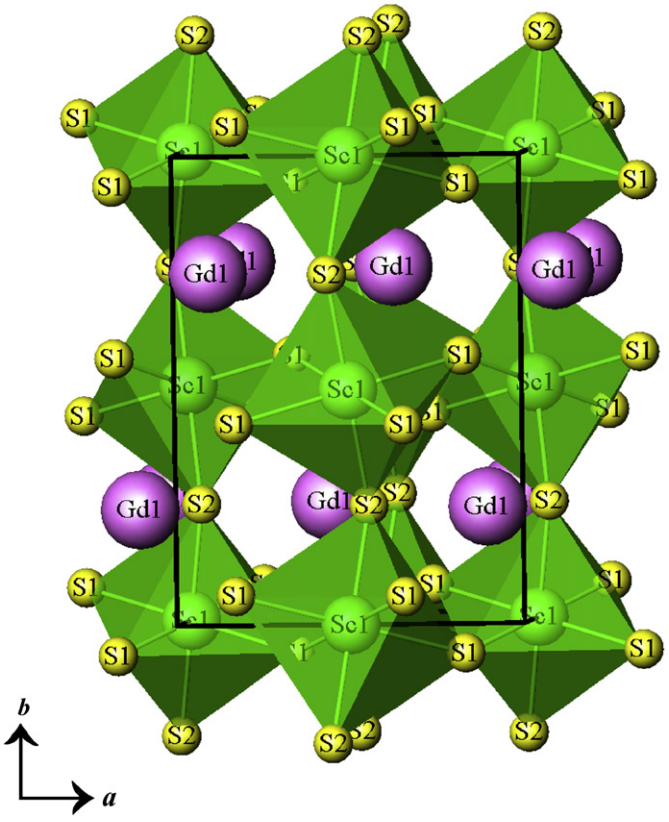

Fig. 2. Three-dimensional channel structure of $GdScS_3$ viewed down the *c* axis. Gd–S bonds have been omitted for clarity.

with six identical units to form three-dimensional channels that are filled by Gd^{3+} ions. Each Gd^{3+} ion is surrounded by eight sulfur atoms in a bicapped trigonal prismatic arrangement (Fig. 3a). The

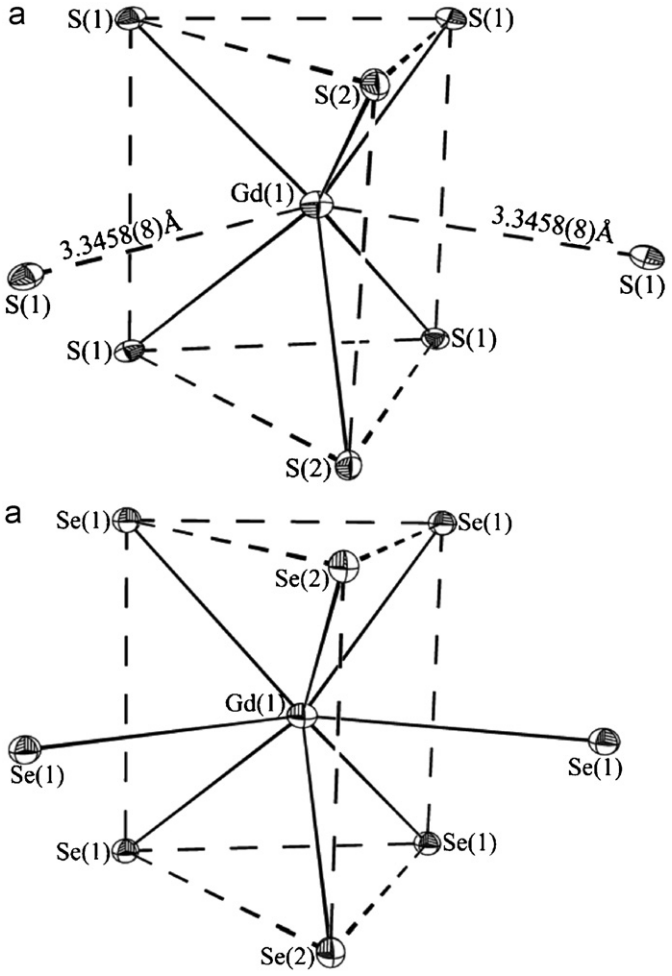

Fig. 3. Illustrations of the coordination environments for Gd^{3+} ions in: (a) $GdScS_3$ and (b) $Gd_{1.05}Sc_{0.95}Se_3$.

two long Gd–S contacts of 3.3458(8) Å are considered as much less important.

The structure of $Gd_{1.05}Sc_{0.95}Se_3$ consists of two-dimensional $ScSe_6$ octahedral layers, which are separated by Gd^{3+} ions (Fig. 4). Within each layer, $ScSe_6$ octahedra share edges along *a* axis and corners along *c* axis with each other. Gd^{3+} ions are eight-coordinate and occur as bicapped trigonal prisms (Fig. 3b).

The selected bond distances for $Gd_{3.04}Sc_{0.96}S_6$, $GdScS_3$, and $Gd_{1.05}Sc_{0.95}Se_3$ are listed in Table 5–7, respectively. They are all normal compared to average values reported by Shannon [26].

3.2. Magnetic susceptibility

Magnetic measurement results for $Gd_{3.04}Sc_{0.96}S_6$, $GdScS_3$, and $Gd_{1.05}Sc_{0.95}Se_3$ are presented in Figs. 5–11. Their effective magnetic moments and Weiss constants obtained by fitting the high temperature susceptibility data into the Curie–Weiss law are listed in Table 8 [34]. As expected for the magnetic behavior of Gd^{3+} ions, all three compounds obey the Curie–Weiss law above their magnetic transition temperatures without any sign of crystal-field effects. The effective magnetic moments are close to calculated values for free Gd^{3+} ions. Their small absolute values of θ_p indicate relative weak magnetic interactions between Gd^{3+} ions.

For $Gd_{3.04}Sc_{0.96}S_6$, the curve of the reciprocal susceptibility bends upward below 9 K, as shown in Fig. 5. No divergence

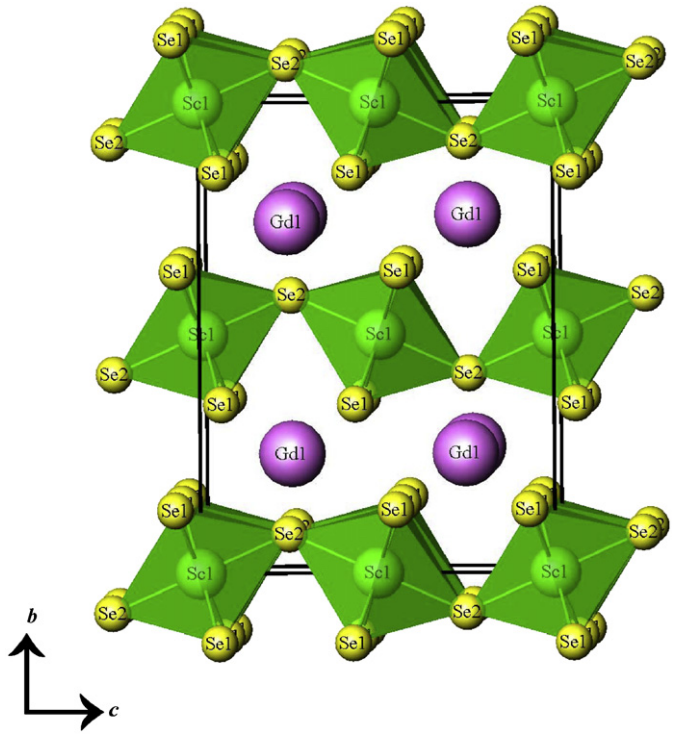

Fig. 4. A depiction the two-dimensional layer structure of $Gd_{1.05}Sc_{0.95}Se_3$ along the *b* axis. Gd–Se bonds have been omitted for clarity.

Table 5
Selected interatomic distances (Å) for $Gd_{3.04}Sc_{0.96}S_6$.

Formula	$Gd_{3.04}Sc_{0.96}S_6$
Gd(1)–S(1)	2.964(1)
Gd(1)–S(2) × 2	2.801(1)
Gd(1)–S(3) × 2	2.858(1)
Gd(1)–S(5)	2.900(1)
Gd(1)–S(6) × 2	2.921(1)
Gd(2)–S(1) × 2	2.880(1)
Gd(2)–S(3)	3.052(1)
Gd(2)–S(4) × 2	2.922(1)
Gd(2)–S(5)	3.136(1)
Gd(2)–S(6) × 2	2.769(1)
Gd(3)–S(2)	2.715(1)
Gd(3)–S(3) × 2	2.754(1)
Gd(3)–S(4) × 2	2.827(1)
Gd(3)–S(5)	2.871(1)
Gd(3)–S(6)	2.884(1)
Gd(4)/Sc(1)–S(1) × 4	2.6142(9)
Gd(4)/Sc(1)–S(2) × 2	2.444(1)
Gd(5)/Sc(2)–S(4) × 2	2.554(1)
Gd(5)/Sc(2)–S(5) × 4	2.5743(9)

Table 6
Selected interatomic distances (Å) for $GdScS_3$.

Formula	$GdScS_3$
Gd(1)–S(1) × 2	2.7830(8)
Gd(1)–S(1) × 2	2.9476(8)
Gd(1)–S(1) × 2	3.3458(8)
Gd(1)–S(2)	2.739(1)
Gd(1)–S(2)	2.751(1)
Sc(1)–S(1) × 2	2.5283(8)
Sc(1)–S(1) × 2	2.5625(8)
Sc(1)–S(2) × 2	2.5436(5)

Table 7
Selected interatomic distances (Å) for $Gd_{1.05}Sc_{0.95}Se_3$.

Formula	$Gd_{1.05}Sc_{0.95}Se_3$
Gd(1)–Se(1) × 4	3.0033(5)
Gd(1)–Se(1) × 2	3.2689(6)
Gd(1)–Se(2) × 2	2.8490(6)
Gd(2)/Sc(1)–Se(1) × 4	2.7192(4)
Gd(2)/Sc(1)–Se(2) × 2	2.6261(4)

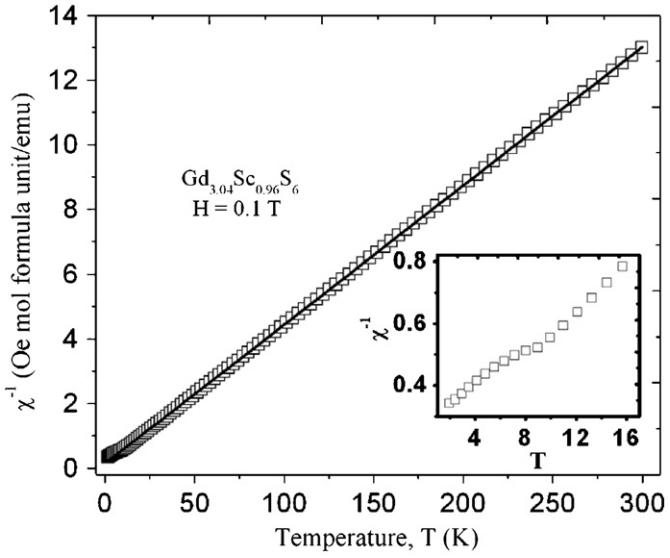

Fig. 5. Inverse molar magnetic susceptibility vs temperature for $Gd_{3.04}Sc_{0.96}S_6$, under an applied magnetic field of 0.1 T between 2 and 300 K. The straight line represents the fit to Curie–Weiss law in the range of 100–300 K. The inset shows the behavior at low temperatures.

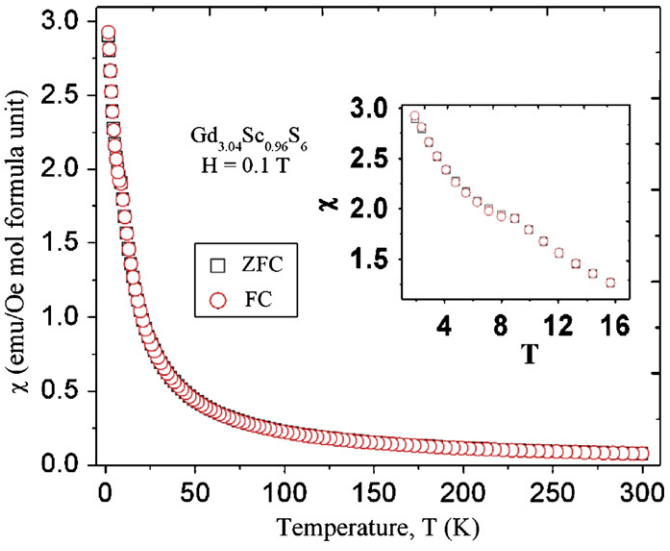

Fig. 6. Molar magnetic susceptibility vs temperature between 2 and 300 K for $Gd_{3.04}Sc_{0.96}S_6$ under ZFC and FC conditions.

observed between ZFC and FC measurements (Fig. 6) and a negative Weiss constant (−3.3 K) suggest an antiferromagnetic nature of the transition at 9 K. Fig. 7 shows the magnetization

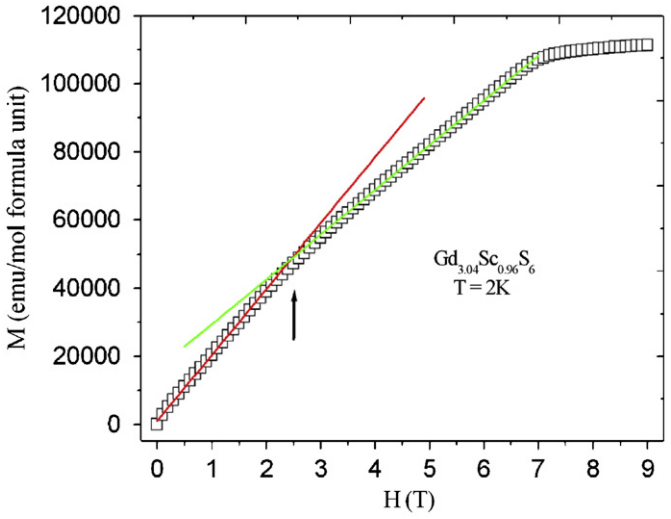

Fig. 7. The magnetization for $Gd_{3.04}Sc_{0.96}S_6$ as a function of applied field at 2 K. Red and green lines are linear fits extended from zero field and from 7 T, respectively. Slight change of the slope and the weak spin reorientation transition field at the junction (up arrow) can be observed.

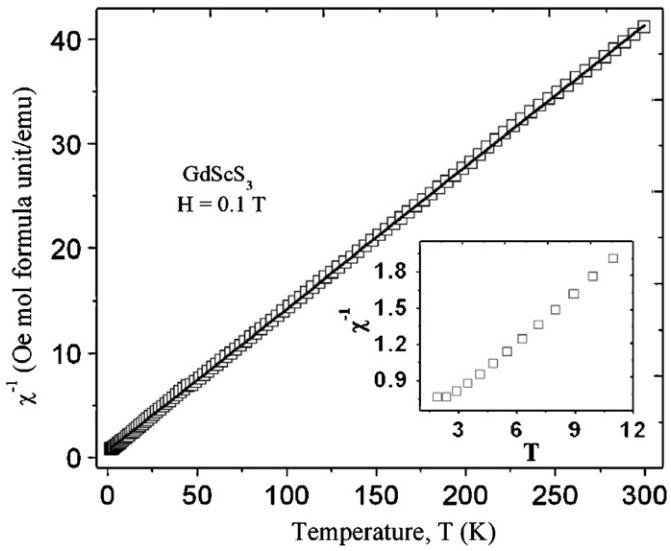

Fig. 8. The temperature dependence of the reciprocal molar magnetic susceptibility for $GdScS_3$ under an applied magnetic field of 0.1 T between 2 and 300 K. The solid line represents the fit to Curie–Weiss law in the range of 100–300 K. Inset shows the reciprocal molar magnetic susceptibilities at low temperature.

measurement at 2 K. There is a spin reorientation transition at $H = 2.5$ T, which is consistent with the antiferromagnetic alignment of the spin. Similar magnetic behavior has been found in another isotypic compound, Gd_3CrSe_6 [35]. The antiferromagnetic ordering of Gd_3CrSe_6 was attributed to the magnetic coupling between Gd^{3+} centers [35].

$GdScS_3$ also exhibits an antiferromagnetic ordering below 3 K, as shown in Fig. 8. The Weiss constant of $GdScS_3$ is −4.5 K. The slight deviation observed during the ZFC–FC measurements (Fig. 9) indicates a ferromagnetic component of the transition caused by canted spin of the Gd^{3+} ions.

Figs. 10–11 shows the temperature dependence of magnetic susceptibility of $Gd_{1.05}Sc_{0.95}Se_3$. The susceptibility increases very rapidly below 5 K indicating a ferromagnetic transition. A positive Weiss constant (1.5 K) and a large divergence observed between

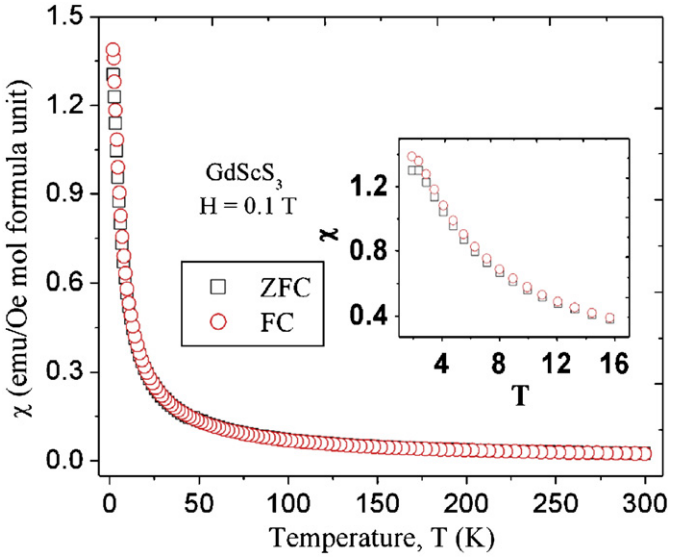

Fig. 9. Variation of molar magnetic susceptibility with temperature between 2 and 300 K for $GdScS_3$ under ZFC and FC conditions.

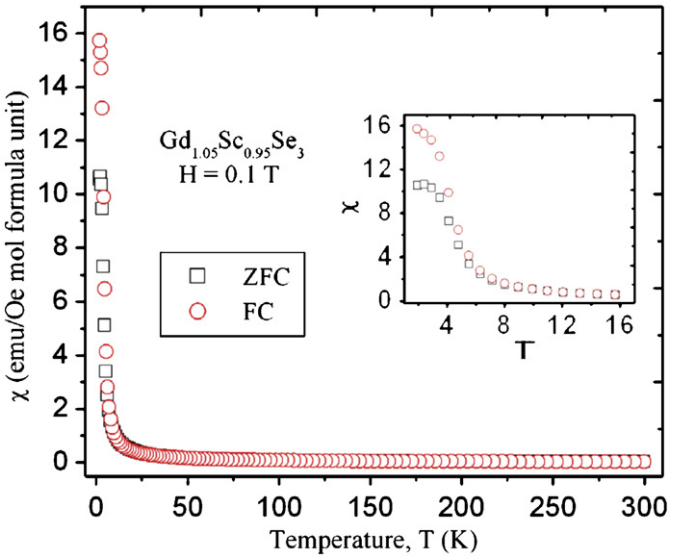

Fig. 11. Molar magnetic susceptibility as a function of temperature for $Gd_{1.05}Sc_{0.95}Se_3$ under ZFC and FC conditions with an applied magnetic field of 0.1 T between 2 and 300 K.

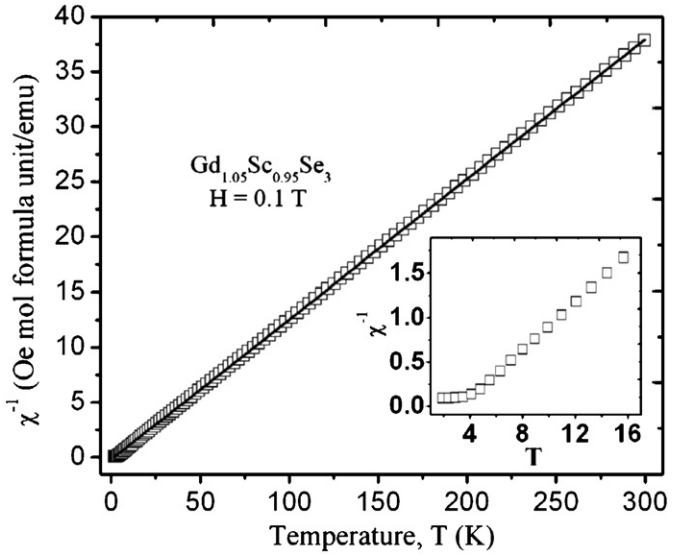

Fig. 10. Inverse molar magnetic susceptibility as a function of temperature for $Gd_{1.05}Sc_{0.95}Se_3$ under an applied magnetic field of 0.1 T between 2 and 300 K. The straight line represents the fit to Curie–Weiss law in the range of 100–300 K. Inset shows the inverse molar magnetic susceptibilities at low temperature.

ZFC and FC measurements are both in agreement with the ferromagnetism.

3.3. Optical properties

Previous studies have shown that the choices of chalcogenides and structures types play important roles in determining the band gaps of interlanthanide chalcogenides [15,19]. This is also true in these gadolinium scandium chalcogenides compounds. As presented in Fig. 12, the band gaps for $Gd_{3.04}Sc_{0.96}S_6$ (dark red), $GdScS_3$ (brown), and $Gd_{1.05}Sc_{0.95}Se_3$ (black) are estimated to be 1.5, 2.1, and 1.2 eV, respectively, from the steepest slope of the absorption edge. These values are consistent with observed colors. $Gd_{1.05}Sc_{0.95}Se_3$ has a much smaller gap than two sulfides due to the higher energy level of 4p(Se) compared to 3p(S) [36,37]. While

Table 8
Magnetic parameters for $Gd_xSc_yQ_z$ (Q = S, Se).

Formula	P_{cal} (μ_B)	P_{eff} (μ_B)	θ_p (K)	R^2
$Gd_{3.04}Sc_{0.96}S_6$	13.84	13.645(3)	−3.3(1)	0.99998
$GdScS_3$	7.94	7.670(8)	−4.5(4)	0.99983
$Gd_{1.05}Sc_{0.95}Se_3$	8.14	7.932(3)	1.5(1)	0.99998

[a] P_{cal} and P_{eff}: calculated [33] and experimental effective magnetic moments per formula unit.
[b] Weiss constant (θ_p) and goodness of fit (R^2) obtained from high temperature (100–300 K) data.

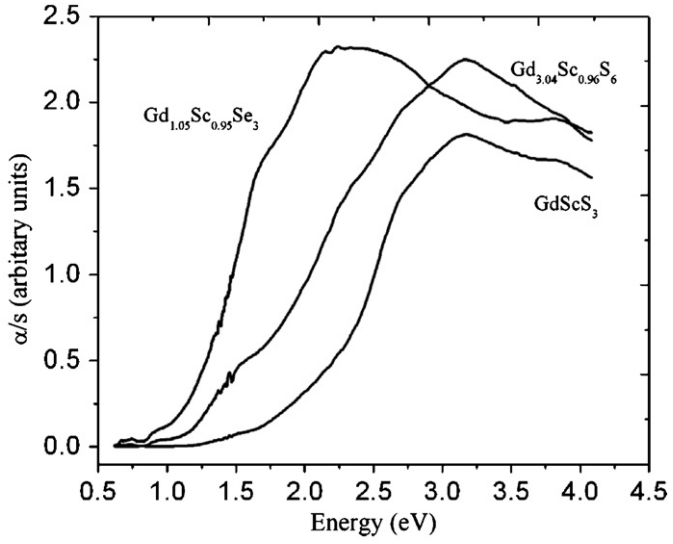

Fig. 12. UV–vis diffuse reflectance spectra of $Gd_{3.04}Sc_{0.96}S_6$, $GdScS_3$, and $Gd_{1.05}Sc_{0.95}Se_3$.

the smaller value for $Gd_{3.04}Sc_{0.96}S_6$ than $GdScS_3$ could be attributed to the its more densely packed structure. The tail below the absorption edge for $Gd_{3.04}Sc_{0.96}S_6$ may indicate an indirect band gap or an impurity like Sb_2S_3.

4. Conclusions

$Gd_{3.04}Sc_{0.96}S_6$, $GdScS_3$, and $Gd_{1.05}Sc_{0.95}Se_3$ have been synthesized and characterized to study the magnetic interactions between Gd^{3+} ions in interlanthanide chalcogenides. All three compounds adopt ordered structure types as intended, although insignificant disorders of Gd/Sc are present in cases of $Gd_{3.04}Sc_{0.96}S_6$ and $Gd_{1.05}Sc_{0.95}Se_3$.

$Gd_{3.04}Sc_{0.96}S_6$, $GdScS_3$, and $Gd_{1.05}Sc_{0.95}Se_3$ exhibit very different magnetic behaviors compared to other interlanthanide analogs. Without the influence of the crystal field, the Weiss constants for these compounds are very small, which indicates weak interactions between Gd^{3+} ions. $Gd_{3.04}Sc_{0.96}S_6$ is an antiferromagnet below 9 K. In contrast, the isotypic compound Ce_3LuSe_6 is a soft ferromagnet with a large negative Weiss constant (−20 K) due to the crystal field splitting of the ground state of the Ce^{3+} ion ($^2F_{5/2}$). $Gd_{1.05}Sc_{0.95}Se_3$ orders ferromagnetically below 5 K. $CeYbSe_3$, $SmYbSe_3$, $PrLuSe_3$, and $NdLuSe_3$ adopt the same structure as $Gd_{1.05}Sc_{0.95}Se_3$, and their magnetic properties have been measured. All are paramagnetic with large negative Weiss constants indicating antiferromagnetic interactions between magnetic ions. $GdScS_3$ ($GdFeO_3$ type) has an antiferromagnetic ordering below 3 K with a weak ferromagnetism. To our knowledge, $GdFeO_3$ type interlanthanide chalcogenides have not been magnetically investigated previously, even though oxide analogs were well studied [38].

Supporting information

X-ray crystallographic files in CIF format for $Gd_{3.04}Sc_{0.96}S_6$, $GdScS_3$, and $Gd_{1.05}Sc_{0.95}Se_3$.

Acknowledgments

This work was supported by the US Department of Energy under Grant DE-FG02-02ER45963 through the EPSCoR Program. Funds for purchasing the UV–vis–NIR spectrometer used in these studies were provided through the Chemical Sciences, Geosciences and Biosciences Division, Office of Basic Energy Sciences, Office of Science, Heavy Elements Program, U.S. Department of Energy under Grant DE-FG02-01ER15187.

Appendix A. Supplementary material

Supplementary data associated with this article can be found in the online version at 10.1016/j.jssc.2009.02.002.

References

[1] N. Rodier, P. Laruelle, C. R. Seances Acad. Sci. Ser. C 270 (1970) 2127.
[2] D. Carré, P. Laruelle, Acta Crystallogr. B 29 (1973) 70.
[3] D.J.W. Ijdo, Acta Crystallogr. B 36 (1980) 2403.
[4] N. Rodier, R. Julien, V. Tien, Acta Crystallogr. C 39 (1983) 670.
[5] N. Rodier, Bull. Soc. fr. Mineral. Cristallogr. 96 (1973) 350.
[6] N. Rodier, R.L. Firor, V. Tien, M. Guittard, Mater. Res. Bull. 11 (1976) 1209.
[7] N. Rodier, V. Tien, C. R. Acad. Sci. Paris Ser. C 279 (1974) 817.
[8] N. Rodier, P. Laruelle, Bull. Soc. fr. Mineral. Cristallogr. 95 (1972) 548.
[9] N. Rodier, P. Laruelle, Bull. Soc. fr. Mineral. Cristallogr. 96 (1973) 30.
[10] F. Hulliger, O. Vogt, Phys. Lett. 21 (1966) 138.
[11] W. Lugscheider, H. Pink, K. Weber, W. Zinn, Z. Ang. Phys. 30 (1970) 36.
[12] P. Lemoine, D. Carre, M. Guittard, Acta Crystallogr. C 41 (1985) 667.
[13] D. Carré, P. Laruelle, Acta Crystallogr. B 30 (1974) 952.
[14] G.B. Jin, E.S. Choi, R.P. Guertin, J.S. Brooks, C.H. Booth, T.E. Albrecht-Schmitt, J. Solid State Chem. 180 (2007) 2581.
[15] K. Mitchell, R.C. Somers, F.Q. Huang, J.A. Ibers, J. Solid State Chem. 177 (2004) 709.
[16] P.E. Dresel, W.B. White, J. Solid State Chem. 177 (2004) 4142.
[17] G.B. Jin, E.S. Choi, R.P. Guertin, J.S. Brooks, T.H. Bray, C.H. Booth, T.E. Albrecht-Schmitt, Chem. Mater. 19 (2007) 567.
[18] G.B. Jin, E.S. Choi, R.P. Guertin, J.S. Brooks, T.H. Bray, C.H. Booth, T.E. Albrecht-Schmitt, J. Solid State Chem. 180 (2007) 2129.
[19] G.B. Jin, E.S. Choi, R.P. Guertin, J.S. Brooks, T.H. Bray, C.H. Booth, T.E. Albrecht-Schmitt, Inorg. Chem. 46 (2007) 9213.
[20] D.L. Gray, B.A. Rodriguez, G.H. Chan, R.P. Van Duyne, J.A. Ibers, J. Solid State Chem. 180 (2007) 1527.
[21] D.L. Gray, D.M. Wells, K. Mitchell, F.Q. Huang, J.A. Ibers, J. Alloys Compd. 441 (2007) 57.
[22] R.P. Guertin, E.S. Choi, G.B. Jin, T.E. Albrecht-Schmitt, J Appl. Phys. 103 (2008) 07B705.
[23] G.B. Jin, E.S. Choi, R.P. Guertin, T.E. Albrecht-Schmitt, J. Solid State Chem. 181 (2008) 14.
[24] M.L. Kahn, J.-P. Sutter, S. Golhen, P. Guionneau, L. Ouahab, O. Kahn, D. Chasseau, J. Am. Chem. Soc. 122 (2000) 3413.
[25] M. Andruh, E. Bakalbassis, O. Kahn, J.C. Trombe, P. Porcher, Inorg. Chem. 32 (1993) 1616.
[26] R.D. Shannon, Acta Crystallogr. A 32 (1976) 751.
[27] G.M. Sheldrick, SHELXTL PC, Version 6.12, An Integrated System for Solving, Refining, and Displaying Crystal Structures from Diffraction Data; Siemens Analytical X-ray Instruments, Inc., Madison, WI, 2001.
[28] G.M. Sheldrick, SADABS 2001, Program for absorption correction using SMART CCD based on the method of Blessing: Blessing, R. H. Acta Crystallogr. A 51 (1995) 33.
[29] L.N. Mulay, E.A. Boudreaux, Theory and Applications of Molecular Diamagnetism, Wiley-Interscience, New York, 1976.
[30] W.W. Wendlandt, H.G. Hecht, Reflectance Spectroscopy, Interscience Publishers, New York, 1966.
[31] N. Rodier, V. Tien, Acta Crystallogr. 32 (1976) 2705.
[32] M. Marezio, J.P. Remeika, P.D. Dernier, Acta Crystallogr. B 26 (1970) 2008.
[33] H. Noël, J. Padiou, Acta Crystallogr. B 32 (1976) 1593.
[34] C. Kittel, Introduction to Solid State Physics, sixth ed., Wiley, New York, 1986.
[35] O. Tougait, J.A. Ibers, Inorg. Chem. 39 (2000) 1790.
[36] A.V. Prokofiev, A.I. Shelykh, A.V. Golubkov, I.A. Smirnov, J. Alloys Compd. 219 (1995) 172.
[37] A.V. Prokofiev, A.I. Shelykh, B.T. Melekh, J. Alloys Compd. 242 (1996) 41.
[38] K. Ito, K. Tezuka, Y. Hinatsu, J. Solid State Chem. 157 (2001) 173.